Title

Shining Light on Carbon Nitrides: Leveraging Temperature To Understand Optical Gap Variations

Journal

Chemistry of Materials, 30(13)

ISSN

0897-4756

Authors

Li, Xiaobo
Melissen, Sigismund TAG
Le Bahers, Tangui
et al.

Publication Date

2018-07-10

DOI

10.1021/acs.chemmater.8b00740

Peer reviewed

Shining Light on Carbon Nitrides: Leveraging Temperature to Understand Optical Gap Variations

Xiaobo Li,[†,‖] Sigismund T.A.G. Melissen,[‡,‖] Tangui Le Bahers,[‡] Philippe Sautet,[¶] Anthony F. Masters,[†] Stephan N. Steinmann,[*,‡] and Thomas Maschmeyer[†,§]

†*Laboratory of Advanced Catalysis for Sustainability School of Chemistry The University of Sydney, Sydney, 2006, Australia*
‡*Université de Lyon, Université Claude Bernard Lyon 1, Ecole Normale Supérieure de Lyon, Centre Nationale de Recherche Scientifique, 46 allée d'Italie, F-69007 Lyon Cedex*
¶*Department of Chemical and Biomolecular Engineering and Department of Chemistry and Biochemistry University of California, Los Angeles Los Angeles, CA 90095, USA*
§*Australian Institute of Nanoscale Science and Techonology, The University of Sydney, Sydney 2006, Australia*
‖*Contributed equally to this publication*

E-mail: stephan.steinmann@ens-lyon.fr,thomas.maschmeyer@sydney.edu.au

Abstract

Polymeric carbon nitride (PCN)-based materials have opened new research avenues in the photocatalytic field. The understanding of parameters underlying the optical properties of PCNs is critical to improve their performance. Herein, the optical properties of PCNs are investigated with a combination of Time-Dependent Density Functional Theory (TD-DFT) calculations and laboratory characterizations, including Variable Temperature (VT)-XRD, VT-UV-Vis and VT-IR techniques, on samples prepared using a broad range of synthesis temperatures. Upon increasing the synthesis temperature from 390 to 600°C, the optical gap E_g^{opt}(eV) narrows from 2.92 to 2.67, and on further increasing the synthesis temperature to 700°C, widens to 3.03 and another absorption at ∼2.2 eV is observed. The TD-DFT calculations show that E_g^{opt} of PCNs converges rapidly with heptazine oligomer size, indicating localized photophysics behavior and justifying a molecular approach. Calculations exploring geometrical variations upon increasing the temperature at which the optical properties were determined revealed that the net effect of these variations were limited, suggesting a vibrational origin of the observed decrease in the gap. The absorption at ∼2.2 eV is tentatively attributed to fully polymerized graphitic PCN oligomers as suggested by the excitation wavelength-dependent photoluminescence emission behavior. The results provide novel insights into the optical properties of PCNs, providing directions for the development of the next generation of PCN-based photocatalysts with optimal light harvesting abilities.

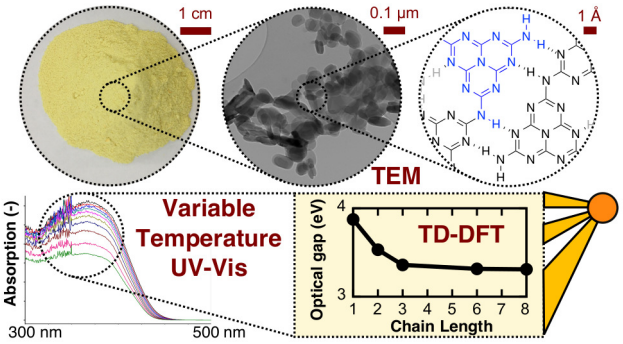

Graphical TOC

1 Introduction

1.1 Polymeric Carbon Nitrides

Polymeric carbon nitrides (PCN)s are an emerging class of polymeric light-absorbers for solar hydrogen production.[1–10] Since the first reported application in photocatalysis in 2009,[1] PCN has been recognized as a very promising photocatalyst component with encouraging efficiencies. Notably, a solar-to-hydrogen efficiency of ∼2.2% with a carbon nitride/carbon dot system[11] and an apparent quantum efficiency of ∼51% for the photocatalytic hydrogen evolution reaction[12] were demonstrated. These efficiencies are amongst the highest reported in combination with dispersed co-catalysts, including those obtained with inorganic semiconductors.[13] The molecular formula, C_3N_4, which is widely used in the literature, represents a fully polymerized graphitic carbon nitride (graphitic PCN) with either tri-*s*-triazine (also called heptazine, *gh*-C_3N_4) or triazine (*gt*-C_3N_4) as repeating units.[14]

Semi-crystalline PCNs are generally prepared by thermal polymerization of precursors, such as cyanamide, urea or melamine. The as-prepared PCN sample often has a C/N ratio of around 0.67, and ∼1 wt% H. Therefore, the structure of this carbon nitride is best represented by the melon model.[15–19] . This model has compositional formula $C_6N_9H_3$. It was first characterized crystallographically by Lotsch et al.[15] and the origins of its stability have been well-described computationally.[20,21] The melon structure is composed of stacked polymer layers of partially condensed heptazine units.

1.2 The Optical Gap of PCNs

Experimentally, PCNs with the melon structure are widely reported to have an optical gap $\mathbf{E_g^{opt}}$ of ∼ 2.7 eV, with a yellow color. Invariably, for both the theoretical and experimental treatment, we will discuss here the optical gap,

$\mathbf{E_g^{opt}}$, as specified in Ref. 22 and occasionally shortened here to "the gap."

As can be seen from the overview recently provided by several of us (*cf.* Fig. 6 in Ref. 23), determining $\mathbf{E_g^{opt}}$ for PCNs is a delicate task. Experimentally, uncertainties exist regarding the exact obtained molecular structure, and whether the phase assumed to dominate is indeed responsible for the measured bandgap. Furthermore, different ways of extracting the gap from experimental data, such as UV-Vis or Photoluminescence spectra, lead to different estimates.

Assuming a Wannier-Mott model in combination with hybrid Density Functional Theory (DFT) as first reported in Ref. 23 allows a computational determination of the bandgap while correcting for the exciton binding energy, leading to a 2.6 eV gap for melon. Such a good agreement with the experimental estimate of 2.7 eV can, however, be (partly) fortuitious. Indeed, Niu *et al.*[24] - in an effort to underpin experimental results - provided a similar value for melon of 2.8 eV, which is likely due to two errors cancelling each other out: the systematic underestimation of any bandgap by a Generalized Gradient Approximation (GGA)[25,26] functional such as used by Niu on the one hand, and the neglect of the (considerable) exciton binding energy on the other. Applying the sophisticated, but computationally demanding, GW-BSE framework to selected PCN structures[27] demonstrated that our invocation of the Wannier-Mott model itself yields an underestimation of the bandgap.

1.3 Refining the Methodology

The localized character of the excitons suggested by our calculations provoked the question whether a molecular approach could be pursued to (1) determine $\mathbf{E_g^{opt}}$ accurately and (2) explain how its value is affected by structural variations. The notion that PCNs' optical properties are largely local is supported in the literature. Recently, Merschjann et al.[28] advanced experimental evidence for this notion, and Butchosa et al.[29] contributed insights from theory. Disagreement exists as to what extent the optical nature of PCNs can be described in terms of a classical semiconductor's, and to what extent it should be considered as an oligomeric aromatic moiety embedded in a molecular solid. It was recently reported that melon derivatives such as dimelem and trimelem, are capable of visible light absorption.[30] This result contrasts with a subsequent study, which claimed that dimelem and trimelem are unable to absorb visible light.[31] Additionally, a reduced optical gap of PCN at 1.90 eV was reported for an amorphous PCN.[32] In order to be suitable for practical applications, it has been predicted that $\mathbf{E_g^{opt}}$ has to lie between 1.8 and 2.1 eV to meet the targeted $\sim$10 % solar to hydrogen efficiency.[33] Hence, to further exploit the photocatalytic efficiency of PCNs, an understanding of the underlying parameters affecting the optical properties of PCNs is highly desirable. Herein, we report a systematic investigation of the optical properties of PCNs with a combination of experimental and theoretical techniques. In particular, adding to the existing body of knowledge[34,35] of the field, variations in synthesis and analysis (UV-Vis, Fourier-Transform Infrared (FTIR), X-Ray Diffraction (XRD)) temperature are exploited to attain a better understanding of these compounds' optical gaps. Using recent theoretical insights into the local nature of the photoexcitation process in these compounds to perform DFT calculations, we demonstrate how the optical gaps of PCNs are determined by a competition between several parameters, such as the number of condensed monomers, the interlayer distance, the slip between stacked layers and hydrogen bonding between chains.

2 Materials and Methods

2.1 Experimental

2.1.1 Instrumentation

PCN polycondensations used a tube furnace (Carbolite, GHA 12/300). Diffuse reflectance UV-Vis spectra were collected on a Varian Cary 5 UV/Vis spectrophotometer equipped with a Praying Mantis chamber. The Variable Tem-

perature (VT) UV-Vis spectra were collected with a CHC reaction chamber (supplied by Harrick). The optical gaps were determined from the diffuse reflectance spectrum using Tauc plots. Surface area and porosity measurements were carried out on a Micromeritics Accelerated Surface Area and Porosimetry System 2020 instrument. Each sample was degassed at 120 °C, and N_2 adsorption/desorption isotherms were collected at -196 °C. The BET surface areas were calculated from the adsorption branch of the isotherms by using the Micromeritics software. Elemental microanalysis was performed on an Elemental Analyzer, Model PE2400 CHNS/O (PerkinElmer, Shelton, CT, USA) with a PC based data system, PE Datamanager 2400 for Windows™ and a PerkinElmer AD-6 Ultra Micro Balance. Powder XRD patterns were collected using a PANalytical X'Pert PRO MPD X-ray diffractometer using Cu Kα (λ = 1.5419 Å) radiation. The VT XRD was performed on a Panalytical Empyrean with an Anton Paar XRK900 high temperature attachment. Measurements were conducted under N_2 with a flow rate of 10 mL/min (Conditions: 45 kV and 40 mA, divergent slit 0.5° and anti-scattering slit 1.0°). Infrared spectra were collected on a Bruker Vertex 80V operating in attenuated total reflectance mode. X-Ray Photoelectron Spectroscopy (XPS) was performed on an ESCALAB250Xi (Thermo Scientific, UK) with source of mono-chromated Al Kα (1486.68 eV). The background vacuum is better than $2 \cdot 10^{-9}$ mbar. VT-IR spectra were collected on a Bruker Hyperion 3000 spectrometer in transmission mode. The sample, suspended in a KBr disc, is placed on Linkam Stage FTIR600 (Linkam Scientific, Surrey, United Kingdom, Zinc Selenide windows (1.0 mm thick)). Spectra were acquired under flowing N_2 with a flow rate of 300 mL/min. The steady-state fluorescence spectra were measured using a Leica SP5 II confocal and multiphoton microscope. The multiphoton excitation wavelength is varied over the range of 690-1060 nm. Samples were ground and placed on a ground steel plate before measurement on a MALDI-TOF mass spectrometer (Bruker autoflex Speed LRF with Smartbeam II laser) in linear mode with 7,7,8,8-tetracyanoquinodimethane as matrix. The laser power was optimized for each sample.

2.1.2 Syntheses of PCNs

All chemicals used were reagent grade and were used as received. The precursor, melamine, was loaded on a lidded alumina boat and heated to different temperatures from room temperature with a ramp rate of 2.2 °C/min in a quartz tube (2.5 cm in diameter) with flowing N_2 gas at a flow rate of 100 mL/min and then held at the desired temperature for 4 h. Essentially, this method using melamine as the precursor compound is inspired by the original synthesis of crystalline melon by Lotsch[15] and subsequent syntheses of other crystalline forms of melon[17] and melon derivatives that have particularly interesting optical features.[30] Each sample is labeled as CNX, where X indicates the synthesis temperature. For example, CN500 is the sample produced from melamine by heating at 500 °C for 4 h. For CN390, the material was kept at 390 °C for 24 h and the resultant white solid (∼5 g) was boiled in 100 ml water with 10 vol% acetic acid. After thoroughly washing with copious amounts of water, the white solid CN390 was dried in an oven at 110 °C overnight. The powder colors ranged from white (CN390), through light yellow (CN450), yellow (CN500, CN550, CN600) to orange (CN650, CN700). Carbon nitride nanosheets (CNNS) were prepared by calcination of CN550 in static air to 550 °C with a ramp rate of 5 °C/min from room temperature and held at 550 °C for 2 h.[10] The CNNS sample is white with a very light yellow hue.

2.2 Computational Methods

All studied structures were optimized following the protocol used in refs. 23 and 27. Time-Dependent Density Functional Theory (TD-DFT)[36] calculations invoking the Tamm-Dancoff Approximation[37] were subsequently performed at the B2PLYP[38] level of theory, with the cc-pVDZ[39] basis set employing the

ORCA package version 4.0.1.2.[40] "Double hybrid" functionals such as the B2PLYP functional used here include second-order Møller-Plesset correlation terms and hence are more computationnally more demanding, than normal hybrid functionals such as B3LYP and simpler GGA functionals such as PBE.[41] Such functionals have been shown to be quite robust and accurate for the calculations of excitation spectra of organic and highly conjugated molecules.[37,42,43] Furthermore, our previous study has shown that this level of theory is in good agreement with reliable EOM-CCSD computations for closely related compounds.[27] Unless specified otherwise, the first optical transition is provided. The Supporting Information (SI) details the numerical settings, §S2.2 as well as some additional calculations using B3LYP and PBE for comparison, §S2.4.

3 Results and Discussion

3.1 Experimental Results

3.1.1 Structural Features

In this study, PCN samples were typically prepared using a high temperature polymerization strategy with melamine as precursor. Synthesis temperatures were varied from 390 to 700 °C, a range which covers the whole synthetic temperature range reported for PCN syntheses in the literature. Fig. 1a contains the XRD patterns of samples prepared at temperatures from 500 to 700 °C. These samples show characteristic patterns of melon.[15,17,18] Two main reflections at $\sim$ 13° and $\sim$ 27.5° are assigned to intralayer periodicity (210) and interlayer periodicity (001), respectively.

Transmission Electron Microscopy (TEM) images show that CN700 has a plate-like morphology (Fig. 1b) and suggest that micro-domains form where the number of condensed monomers typically lies in the order range of 10^1 to 10^4, suggesting that whereas edge effects probably matter for their photophysical behavior, polymer length itself would not.

All samples have similar C/N ratios of $\sim$0.67 and $\sim$1 wt% H content from elemental analysis (Fig. 2 and Table S1). The C/N ratio is consistent with the theoretical one found for melon, but the hydrogen content is below the theoretical value of 1.53% for synthesis temperatures higher than 450°. This deviation is probably due to the incomplete combustion during elemental analysis. The BET surface areas of CN500, CN550, CN600, CN650 and CN700 are 10, 15, 26, 31 and 33 m^2/g, respectively. The surface areas gradually increase with increased synthesis temperature (Fig. 2), with smaller PCN particles being created at higher temperatures. FTIR and Raman spectra of all samples show similar spectra, containing the characteristic vibration absorption spectra of PCN (Fig. S1).[44] Lower synthesis temperatures of 450 and 390 °C result in two crystalline materials (Fig. S2), mainly composed of melem and its oligomers, such as dimelem and trimelem, as suggested by elemental analysis (Table S1) and Matrix-Assisted Laser Desorption/Ionization - Time of Flight (MALDI-TOF) (Fig. S3 m/z 420, 621). The theoretical C/N ratios of melem ($C_6N_{10}H_6$), melon ($C_6N_9H_3$), and C_3N_4 are 0.6, 0.67 and 0.75, respectively. The CN390 and CN450 samples have C/N atomic ratios of 0.60 and 0.62, respectively, close to that of molecular melem. The XRD patterns of PCNs from variable synthesis temperatures show a clear shift of the (001) reflection from 27.50° to 27.95° with increasing synthesis temperature (inset of Fig. 1a). This indicates a decrease of the interlayer distance from 3.24 to 3.19 Å with the increase of synthesis temperature. Conversely, over the same range of synthesis temperatures, the reflection at $\sim$13° shifts to 12.8° indicating the increase of the repeat distance along the hkl-plane (210), i.e., within the layers. Additionally, the Full Width at Half Maximum (FWHM) of the (001) reflection decreases with increased synthesis temperature from 1.21° to 0.58°, suggesting an increased crystallinity domain along the (001) direction. The sharpening of the (210) reflection observed in the XRD patterns of samples prepared over the synthesis range from 500 to 700 °C.

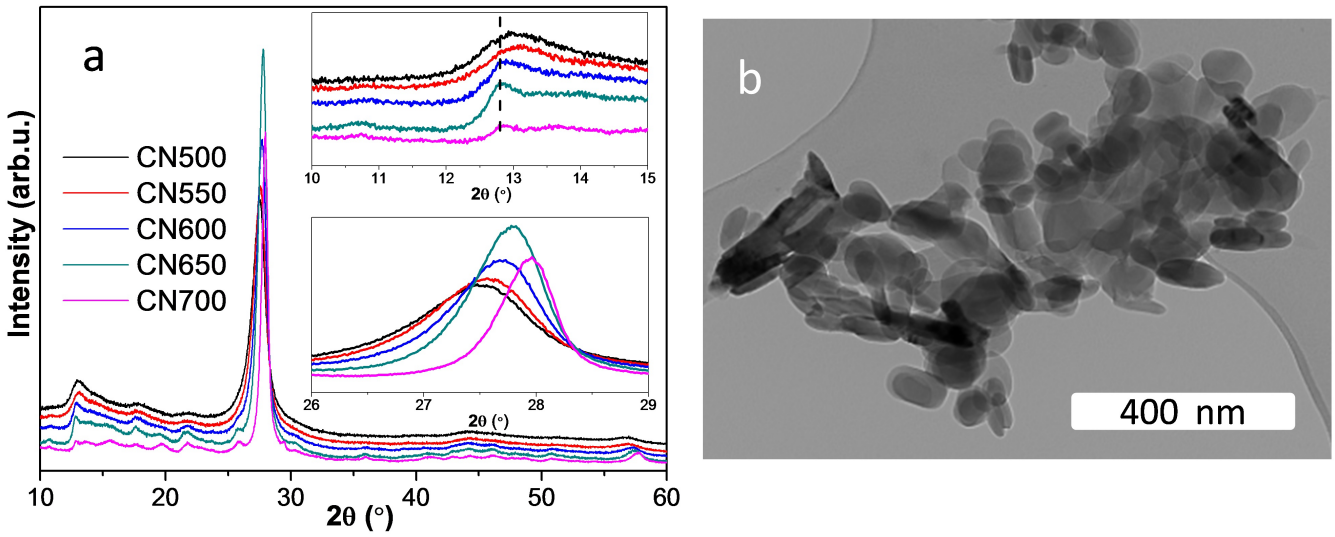

Figure 1: XRD patterns of PCN synthesized at different temperatures (a) and TEM images of CN700 sample (b).

3.1.2 General UV-Vis Results

Fig. 3a illustrates the solid UV-Vis diffuse reflectance spectra of the PCN samples. For those samples prepared with synthesis temperatures in the range from 390 to 550 °C, the main absorption shifts to long wavelength as the synthesis temperature is increased. With a further increase of synthesis temperature, a blue-shift of the main absorption band is observed. The optical gaps of PCN (Fig. 2 and Table S1) are calculated from the diffuse reflectance spectra using the Tauc plots. The gaps follow a decreasing trend from 2.92 to 2.67 eV, then increase to 3.03 eV as the synthesis temperature increases.

The literature indicates that PCN samples with a melon structure have optical gaps of ∼2.7 eV. This is consistent with our observation that CN500, CN550 and CN600 have optical gaps of ∼2.7 eV. However, the gap increases from ∼2.7 eV to ∼3.0 eV for CN650 and CN700 samples, which is unexpected. The elemental analysis and IR results suggest similar compositions to those synthesized at lower temperatures. The variable gaps of PCN samples are probably due to microstructural variations, as detailed in the following.

3.1.3 Variable Temperature Analysis

VT XRD (VT-XRD) and UV-Vis (VT-UV-Vis) were performed on the CN500 and CN650 samples (Fig. 4). The (001) reflections and the UV-Vis absorptions of CN500 and CN650 are found to be temperature-dependent. With the increase of VT-XRD temperature from 25 to 300 °C, continuous shifts of the (001) reflections to low angle are observed on both CN650 and CN550 samples (Fig. 4a, b). This indicates an increased interlayer distance when increasing VT-XRD temperature. In contrast to the shift in the (001) reflection, negligible changes to other reflections are observed. In VT-UV-Vis experiments, the main absorption continuously shifts to long wavelength with increasing temperature (Fig. 4c, d). Combining VT-XRD and VT-UV-Vis data, correlations between interlayer distance and $\mathbf{E_g^{opt}}$ of CN650 and CN500 are established such that they increase with the decrease of interlayer distance (Fig. 4e, f). This appears consistent with the widening of $\mathbf{E_g^{opt}}$ observed for CN650, and CN700 samples, which have shorter interlayer distances compared to samples prepared at lower synthesis temperatures. However, several issues ensue from this explanation: first, the gaps of CN500 and CN650 do not cross over when the interlayer distances of CN500 and CN650 cross over in the several VT temperatures (Fig. 4e,f).

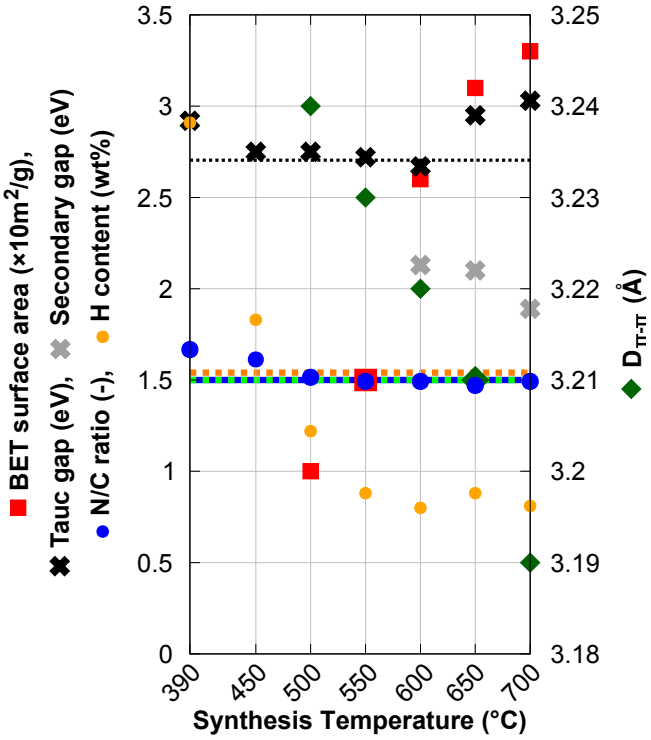

Figure 2: Summary of Table S1. The primary properties of the materials are reported as a function of synthesis temperature. The BET surface area[45] is a measure of the density of photocatalytically active material. The Tauc and secondary gaps are the most important optical qualities of the material. The elemental analysis is provided directly from experiment in terms of the N/C ratio and H content (wt%). $D_{\pi-\pi}$ refers to the interlayer distance. Theoretical values for melon marked with colored lines (in particular $\mathbf{E_g^{opt}}$, H content, $D_{\pi-\pi}$, and N/C ratio (the latter two superimposed) are marked .

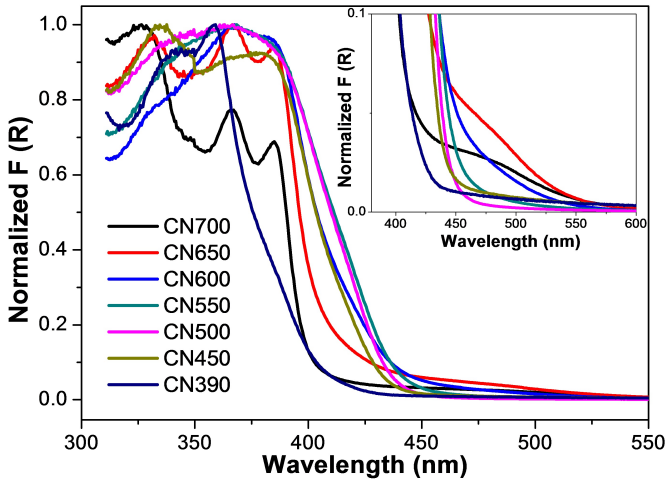

Figure 3: Normalized UV-Vis diffuse reflectance spectra of PCN samples synthesized at different temperatures.

Second, with the variable temperature XRD and UV-Vis experiments on the CN650 sample, a continuous decrease of $\mathbf{E_g^{opt}}$ over an interlayer distance range from 3.28 to 3.21 Å is observed. However, for the PCN samples synthesized at variable temperature their optical gaps follow the trend of decreasing then increasing from ∼2.9 to ∼2.7 then to ∼3.0 eV as the interlayer distance varies over a similar distance. Third, a smaller gap change (∼0.1 eV per 0.07 Å) of CN650 and CN500 in VT experiments is observed compared to the ∼0.3 eV difference, over a similar variation in interlayer distance, observed on PCN samples synthesized at other temperatures. The combination of these observations strongly suggests that there are other microstructural parameters affecting the gap of PCN samples.

Another UV-Vis absorption feature is the appearance of a more noticeable shoulder at ∼570 nm in the spectra of samples synthesized at temperatures in excess of 600 °C (inset of Fig. 3). In the spectra of samples synthesized at temperatures of 600, 650 and 700 °C, second, narrower gap features can be calculated at 2.13, 2.10 and 1.89 eV (Table S1), respectively.

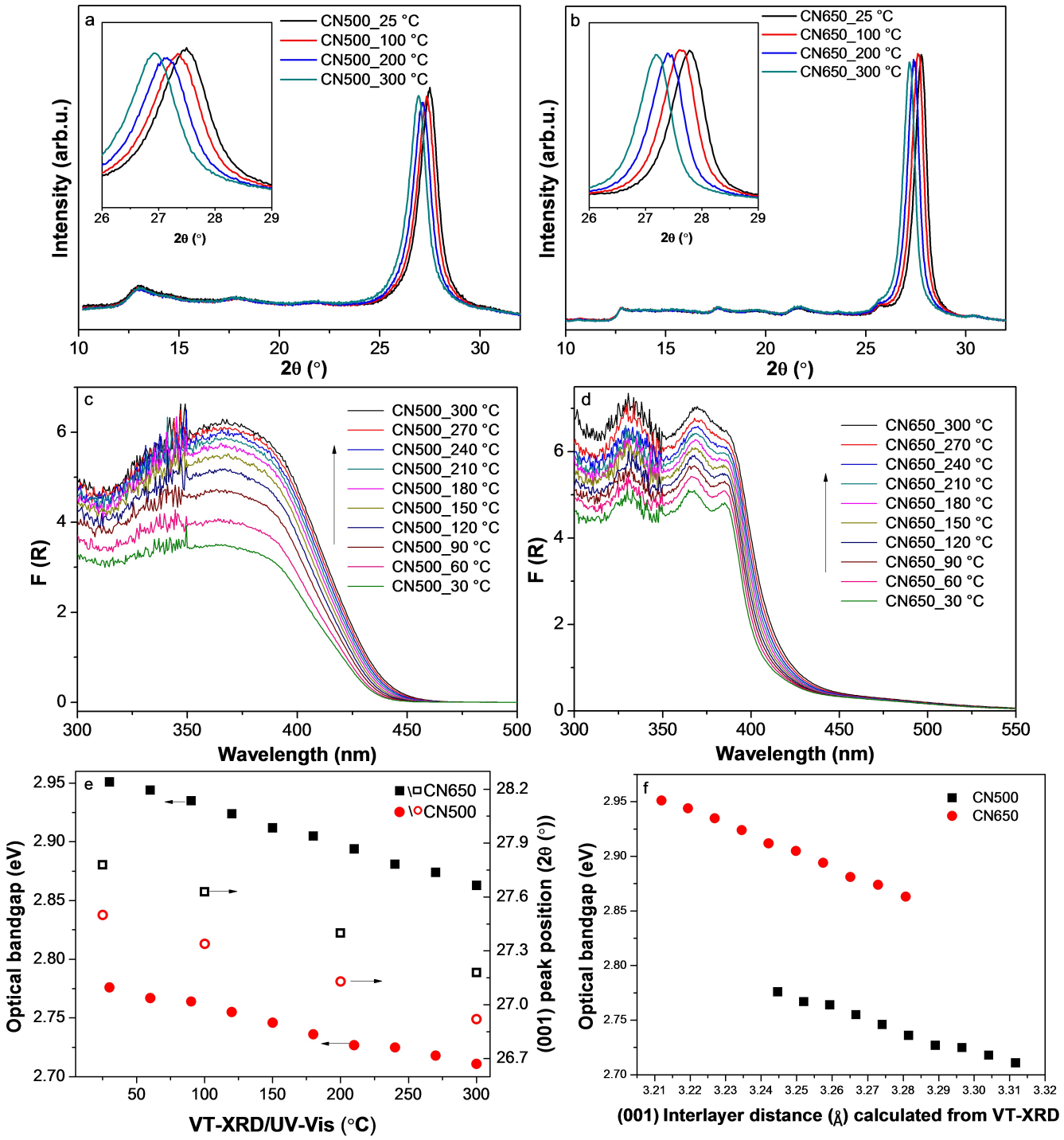

Figure 4: VT-XRD of CN500 (a) and CN650 (b); VT-UV-Vis of CN500 (c) and CN650 (d); temperature-dependent variation of $\mathbf{E_g^{opt}}$ and (001) reflections of CN500 and CN650 in VT-XRD and VT-UV-Vis experiments (e). Correlation between $\mathbf{E_g^{opt}}$ and (001) interlayer distances (f). The additional data in interlayer distances are calculated from VT-XRD.

3.1.4 Photoluminescence

Fig. 5 illustrates the photoluminescence (PL) spectra of samples. PL spectra show a main emission centered at ∼459 nm, and a second emission at ∼505 nm with tails to 650 nm. The emission at ∼459 nm is assigned to conduction-valence band relaxation. Interestingly, excitation-dependent PL studies show that the 505 nm emissions depend on the synthesis temperature (Fig. S4). The 505 nm emis-

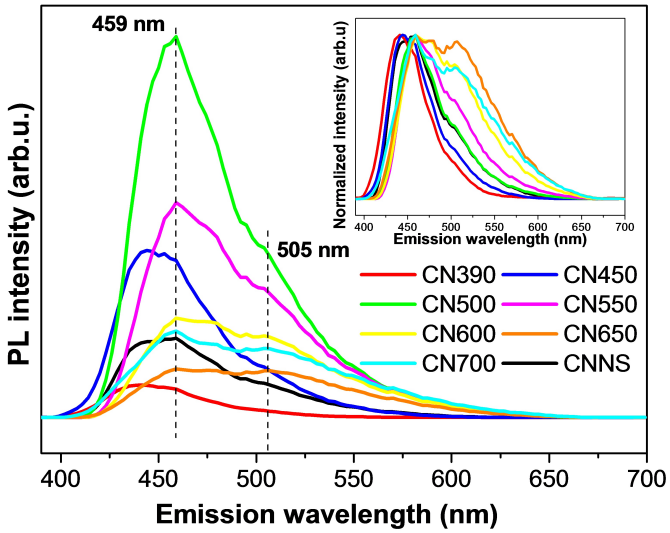

Figure 5: Photoluminescence of PCN samples with two photon excitation at 720 nm. Normalized spectra are shown in the inset.

sions of PCN samples synthesized between 390 and 550 °C are not excitation-dependent. By contrast, this emission is found to be excitation-dependent on CN600, CN650 and CN700 samples. This indicates that the processes behind the 505 nm emissions are different for those samples.

3.2 Computational Results

3.2.1 Chromophore Variations

The PCN synthesis is best understood as a series of cyclizations of triazine rings and polymerizations.[21] Several key systems relevant to this process were studied individually to understand how a melem-based system would compare, generally speaking, to other systems (Fig. 6).

Cyclization, i.e., going from a triazine to a heptazine core, lowers $\mathbf{E_g^{opt}}$ significantly more than condensing two melamines to melam. Melem-based PCNs do not only have lower gaps than melamine based ones, but is also justified by previous spectroscopic information and by earlier calculations performed by several of us[21] that demonstrate the particular stability of melem-based PCNs.[20]

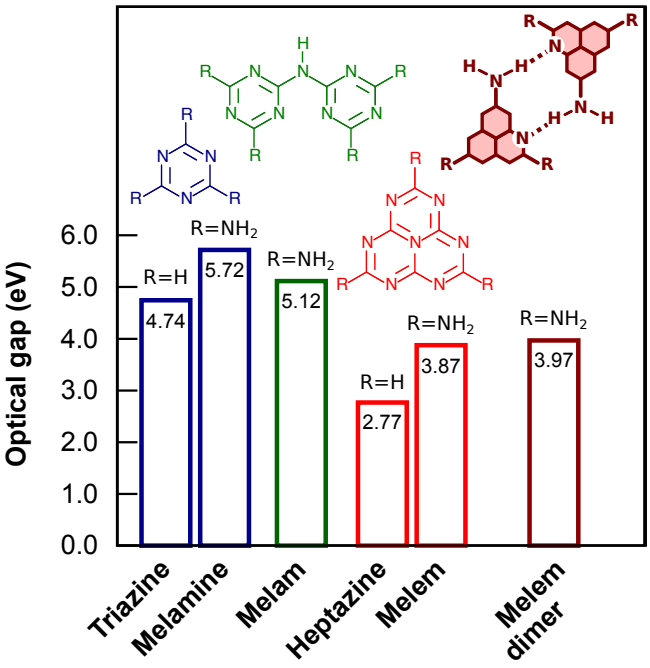

Figure 6: $\mathbf{E_g^{opt}}$ calculated with TD-DFT for a selection of systems.

3.2.2 Effect of System Size

Fig. 7a and Fig. 7b show that the gap of melem oligomers converges rapidly with oligomer size. A control calculation stacking two trimers in a parallel-displaced configuration demonstrates a small lowering of the bandgap of 0.06 eV, essentially confirming the result obtained by stacking two monomers, which yields a similar lowering of 0.04 eV. This convergence at a small system size yields the important insight that the photoexcitation process in PCNs is a localized process, essentially involving the nearest neighbors.[7,21,23,28,29]

This is consistent with the high exciton binding energies, characteristic of localized excitons, reported previously.[23]

3.2.3 Macromolecular Variations and Temperature

It is known[46–48] that $\mathbf{E_g^{opt}}$ is temperature-dependent, decreasing with increasing interatomic spacing and thermal motion. For this reason, in Fig. 8a the H-bond distance is increased stepwise for a a stacked pair of H-bonded melem dimers and the gap computed, showing such a decrease. Replacing –H

with $-NH_2$ will typically cause a bathochromic shift,[49] because the N lone pair is included in the extended π-aromatic network. However, in some instances it will cause a hypsochromic shift.[50] Indeed, Fig. 6 shows that this is the case here, both, when triazine is substituted to melamine and when going from heptazine to melem the gap increases by roughly 1 eV. A further small increase in gap (0.1 eV) is noticed upon H-bonding between two melem dimers (melem dimer in Fig. 6). Upon decreasing the polarization induced by H-bonding by separating the stacked monomers from each other (Fig. 8a, $\mathbf{E_g^{opt}}$ decreases to 3.3 eV, also obtained for a stacked dimer in Fig. 8b.

In Fig. 8b, the qualitative effects of both rotation and interlayer spacing were explored. These effects are best understood invoking an exciton coupling model: depending on the orbital overlap between the two aromatic systems, the coupling is large ("bonding" overlap) or zero ("non-bonding" overlap). At large interlayer distances, no coupling is observed and the relative rotation does not influence $\mathbf{E_g^{opt}}$. Similarly, at a relative rotation of 30°, the HOMO orbital happens to be non-bonding with respect to the two monomers, minimizing the coupling and hence the distance dependence of $\mathbf{E_g^{opt}}$. At relative rotations of 0° and, to a lesser extent, of 60°, the coupling is "bonding" and the gap is lower for smaller interlayer spacings. Hence, increasing the interlayer distance in itself increases $\mathbf{E_g^{opt}}$. Finally, Fig. 8c shows that sliding the monomers away from the hypothetical sandwich-stacking configuration increases the gap due to a decrease in overlap between the aromatic systems. This also implies that the nearest neighbors of the light-absorbing dimer do not have a significant impact on the gap, similar to the situation for the polymerization degree within one chain (Fig. 7). Equivalent conclusions to those based on results displayed in Fig. 8b can be reached from fully optimizing dimers while varying only the strength of the dispersion interaction between two stacked dimers (see SI § S2.1). Finally, a comparison of B2PLYP's performance with that of the two functionals typically used in the literature, B3LYP and PBE, is provided in SI § 2.4.

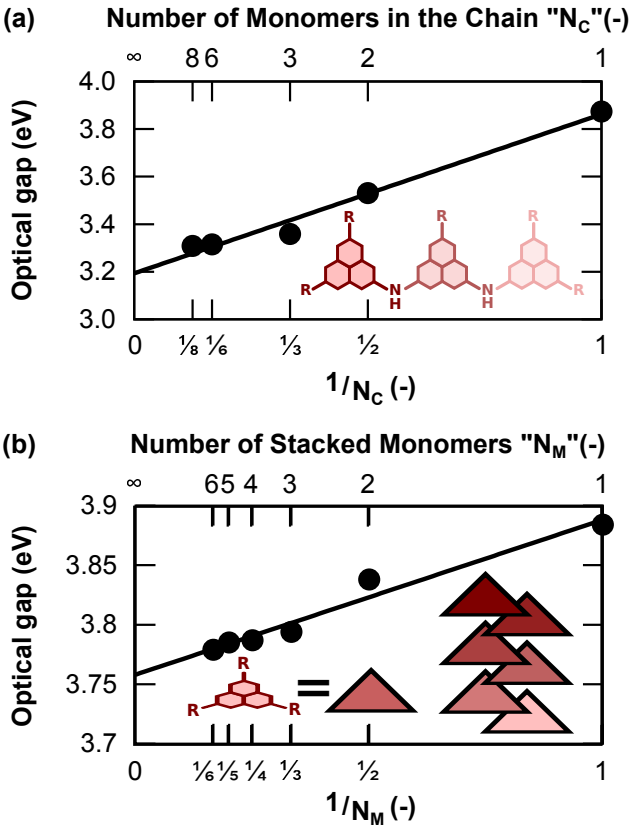

Figure 7: Convergence of $\mathbf{E_g^{opt}}$ calculated using TD-DFT with system size. A linear fit of $\mathbf{E_g^{opt}}$ against the inverse of the number of monomers yields a good estimate of the convergence values. Invariably, R=NH_2. (a) Convergence upon increasing the number of condensed monomers. Convergence value estimated at 3.20 eV. (b) Convergence upon increasing the number of vertical, parallelly-displaced stacked monomers. Convergence value estimated at 3.76 eV. Tabulation of values provided in SI, §S2.3

3.3 Discussion

The above results suggest that the parameters governing $\mathbf{E_g^{opt}}$ of the PCN samples are distinct from typical semiconductor photophysics. The variations, mainly in microstructure, such as the number of condensed monomers, interlayer distances, relative sliding of planes and H-bonds, should be considered for a deep understanding of the overall optical properties of

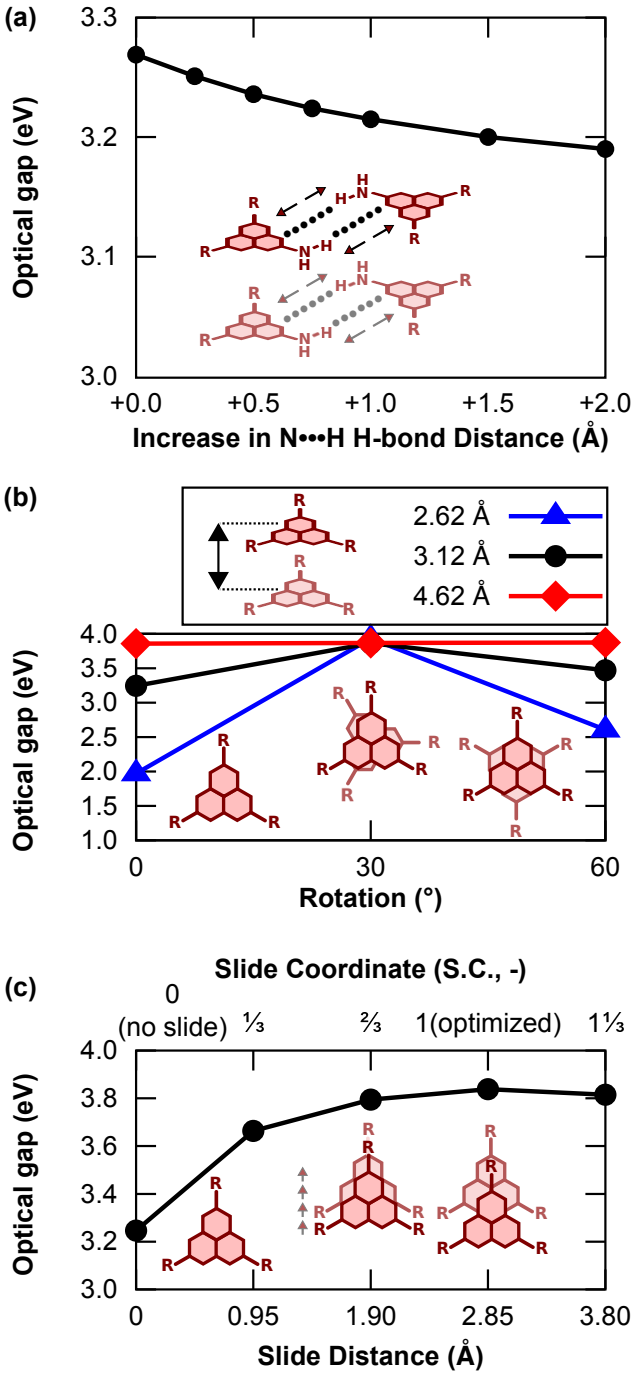

Figure 8: $\mathbf{E_g^{opt}}$ calculated using TD-DFT. Invariably, R=NH_2. (a) Variation of $\mathbf{E_g^{opt}}$ with different N···H H-bonding distances: sandwich stacking configuration, 3.12 Å vertical spacing (equilibrium configuration in the crystal), 2.07 Å N···H spacing at equilibrium (distances expressed with respect to deviation from that distance). (b) Sandwich-stacked melem dimers (c) Parallel displaced melem dimers, with vertical spacing fixed to 3.12 Å and parallel displacement at equilibrium (S.C. = 1) equal to 2.85 Å. Tabulated values in SI, section S2.3

PCN.

The TD-DFT calculations demonstrate that the optical gaps of melem-chains decrease noticeably with increasing numbers of condensed monomers up to 3. This could explain the decreasing optical gap of PCNs synthesized at temperatures from 390 to 450 °C, as elemental analysis suggests an increased oligomer size. However, the oligomer size effect could not explain the optical properties of PCNs synthesized between 500 and 600 °C, as TD-DFT calculations reveal that the gap converges rapidly after 3 monomers, and more importantly, the experimentally measured C/N atomic ratios of ∼0.67 suggest an infinite polymer chain size according to the melon model. Thus, the narrowing of the gap is mainly attributed to the decreased interlayer distance, coherent with our calculations that predict a considerable narrowing of the gap upon decreasing the interlayer distance alone.

The optical gaps of these PCNs widen from 2.67 to 3.03 eV as the synthesis temperature further increases from 600 °C to 700 °C, with the major microstructural change observed being the decrease in the interlayer distance. However, as discussed above this widening cannot be explained by the decreased interlayer distance, because that would be inconsistent with the results from VT-XRD and VT-UV-Vis experiments In addition, the relationship between interlayer distance and $\mathbf{E_g^{opt}}$ revealed by the calculations is further evidence against this explanation.

The TD-DFT study on the geometrical slide effects on the PCN bandgaps sheds light on the underlying photophysics. A 0.5 eV increase of the gap is predicted when stacked dimers slide past each other from the arbitrarily set "slide coordinates" 0 (sandwich stacked) to 1 (optimized geometry, parallel displaced configuration).

It has been suggested that distortions in those PCN samples with the melon structure, such as the different stackings, the shrinking or buckling of the layers, are introduced into the samples by high temperature treatment.[16–18,44] These distortions try to minimize the electron cloud repulsion of tri-*s*-triazine rings induced by reduced interlayer distances. Structurally, the

distortions cause the sliding of layers as modeled in our calculations. Although the relative sliding is not easily quantifiable using XRD, the change in intensity between the (001) and (210) reflections, and the shift of the (210) as a function of synthetic temperature could be the indications of sliding at high synthetic temperatures.[17,18] Therefore, the widening gap of CN650 and CN750 observed in this study is attributed to the geometrical slide effect between the layers, which counteracts the interlayer distance effect, on the gap of PCN. In the VT-UV-Vis experiments, the observed temperature dependence of the gaps is attributed to the increase in interatomic spacing due to the elongation of chemical bonds, particularly the H-bonds in PCN, with increased measurement temperature. The disappearance/broadening of absorptions at 3000 to 3400 cm^{-1} in the VT-IR experiments supports the interpretation of a weakening of the H-bonds of PCNs with increased measurement temperature (Fig. 8). This is also in agreement with the calculation on the effect of the H-bonds distance on the gap. All of the foregoing discussion strongly suggests

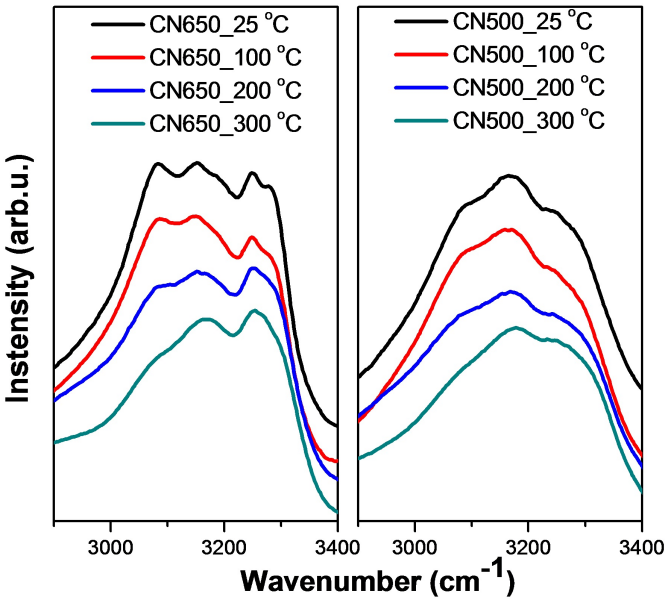

Figure 9: VT-IR spectra of CN650 and CN500.

that the optical properties of the PCN samples result from a combination of (sometimes competing) effects, including the number of condensed monomers, interlayer distances, geometrical sliding of layers and changes in the H-bond distances. Microstructure variations, induced by the synthesis temperature, are the dominant factor in the observed increase of $\mathbf{E_g^{opt}}$ for CN650 and CN700 samples compared to those of samples synthesized at lower temperatures.
The origin of the absorption shoulder at ∼570 nm is inferred here to be the formation of secondary absorption sites, possibly patches of fully polymerized carbon nitride (*gh*-C_3N_4), at high temperatures.[35] Our previous calculations evidence that the optical gap of PCN narrows as further polymerization yields C_3N_4.[23] Another possible reason for the existence of this shoulder could be the mere loss of $-NH_2$ end groups at high temperature:[51] our calculations show that -NH_2 end groups increase the gap and their loss at high temperatures could narrow it (Fig. 6). The authors underline that the notion of certain defects in the carbon nitride structure enhancing the photocatalytic activity - which a redshift of the bandgap would certainly do - is well described in the literature.[8,52] This conclusion is supported by the results of a white-color PCN with nanosheet morphology (Carbon nitride nanosheets (CNNS)),[10] which shows similar composition and structure to those of other PCN samples (Fig. S1, S5-6 and Table S1). The 3.0 eV gap of CNNS (Fig. S7) can be explained similarly to the CN700 sample. In the CNNS sample, the species responsible for the adsorption shoulder were apparently oxidatively removed during CNNS formation, explaining the absence of the absorption shoulder compared to the spectrum of CN700.
The excitation-dependent photoluminescence (PL) is probably due to the presence of different sizes of oligomers with polyheptazine imide[53] or *gh*-C_3N_4 units, which forms multiple states in the gap of PCNs.[54] These states are absent in CNNS (Fig. 5, Fig. S4).

4 Conclusions

Relying on a combination of experimental and theoretical characterizations we show that the optical properties of polymeric carbon nitrides PCNs are determined by a cumulative effect

of many parameters, including the number of condensed monomers, the exact configuration of the H-bonding network, interlayer distances and relative sliding between layers. The overall optical gap $\mathbf{E_g^{opt}}$ of PCN is, thus, a result of the competition between these parameters. This explains the changes in $\mathbf{E_g^{opt}}$ for different synthesis temperatures. Our studies indicate that to develop PCN melon samples with enhanced light harvesting ability, an A-A stacking PCN with decreased interlayer distance is a desirable target.

Density Functional Theory computations were used to discern the individual effect that each experimental parameter has on the gap, arguably the crucial property of these materials for the stated purpose.

Qualitatively, we confirm earlier reports that the heptazine motif gives rise to narrow gaps compared to other species in the same family. A rapid convergence of $\mathbf{E_g^{opt}}$ with oligomer size suggests that the PCN photoabsorption process is highly localized, and that the increased degree of polymerization associated to higher synthesis temperatures has a limited effect individually on $\mathbf{E_g^{opt}}$. However, at synthesis temperatures above 600°C a secondary gap is observed, while the primary Tauc gap increases compared to the lower synthesis temperatures. Hence, at high temperatures, a qualitatively different chemistry, such as structural degradation, or the formation of patches of fully polymerized *gh*-C_3N_4 is probably responsible for the emerging gap of around 2 eV.

A clear, positive correlation between measurement temperature and interlayer spacing was found, whereas the correlation between measurement temperature and $\mathbf{E_g^{opt}}$ was found to be negative. Increasing the interlayer spacing computationally increases the gap, due to a reduced exciton coupling. Hence, the observed decrease in $\mathbf{E_g^{opt}}$ upon heating a given sample must be due to excited vibrational modes and the observed correlation with the interlayer spacing is fortuitous, simply because both are directly correlated to the measurement temperature. The insight into the optical properties of PCNs gained from this study are of potential use to develop tailored synthesis protocols for specific applications and thus to increase the scale at which these polymers are currently deployed in photocatalytic cells.

Acknowledgement We thank Peter Southon for the help on the VT-UV-Vis experiments. We thank Joonsup Lee (The Vibrational Spectroscopy Core Facility) for the help on the VT-IR experiments. We gratefully acknowledge support from the Australian Research Council. STAGM and SNS gratefully acknowledge the computational resources provided by *l'Institut du Développement et des Ressources en Informatique Scientifique* (IDRIS, under project x2015080609) of the *Centre National de la Recherche Scientifique (CNRS)* and by the *Pôle Scientifique de Modélisation Numérique (PSMN)* at ENS Lyon.

Supporting Information Available: Table of elemental analyses, interlayer distance, and optical gap as a function of synthesis temperature; IR-ATR and Raman spectra; X-Ray Photoelectron Spectroscopy (XPS) spectra; additional XRD patterns; MALDI-TOF spectra; two-photon PL-spectra; nanosheet background information; additional DFT calculations on stacking distance effect on $\mathbf{E_g^{opt}}$; additional numerical settings for DFT calculations; numerical values Figures 7 and 8, comparative $\mathbf{E_g^{opt}}$ calculations with the B3LYP and PBE functionals; calculated structures in `.xyz`-format. This material is available free of charge via the Internet at `http://pubs.acs.org/`.

List of Acronyms

CNNS Carbon nitride nanosheets

DFT Density Functional Theory

FTIR Fourier-Transform Infrared

FWHM Full Width at Half Maximum

GGA Generalized Gradient Approximation

MALDI-TOF Matrix-Assisted Laser Desorption/Ionization - Time of Flight

PCN Polymeric carbon nitrides

PL photoluminescence

SI Supporting Information

TD-DFT Time-Dependent Density Functional Theory

TEM Transmission Electron Microscopy

VT Variable Temperature

XPS X-Ray Photoelectron Spectroscopy

XRD X-Ray Diffraction

References

(1) Wang, X.; Maeda, K.; Thomas, A.; Takanabe, K.; Xin, G.; Carlsson, J. M.; Domen, K.; Antonietti, M. A Metal-Free Polymeric Photocatalyst for Hydrogen Production from Water Under Visible Light. *Nature Mater.* **2009**, *8*, 76–80, DOI: 10.1038/nmat2317.

(2) Thomas, A.; Fischer, A.; Goettmann, F.; Antonietti, M.; Müller, J.-O.; Schlögl, R.; Carlsson, J. M. Graphitic Carbon Nitride Materials: Variation of Structure and Morphology and Their Use as Metal-Free Catalysts. *J. Mater. Chem.* **2008**, *18*, 4893–4908, DOI: 10.1039/B800274F.

(3) Wang, X.; Blechert, S.; Antonietti, M. Polymeric Graphitic Carbon Nitride for Heterogeneous Photocatalysis. *ACS Catal.* **2012**, *2*, 1596–1606, DOI: 10.1021/cs300240x.

(4) Wang, Y.; Wang, X.; Antonietti, M. Polymeric Graphitic Carbon Nitride as a Heterogeneous Organocatalyst: from Photochemistry to Multipurpose Catalysis to Sustainable Chemistry. *Angew. Chemie - Int. Ed.* **2012**, *51*, 68–89, DOI: 10.1002/anie.201101182.

(5) Li, X.; Hartley, G.; Ward, A. J.; Young, P. A.; Masters, A. F.; Maschmeyer, T. Hydrogenated Defects in Graphitic Carbon Nitride Nanosheets for Improved Photocatalytic Hydrogen Evolution. *J. Phys. Chem. C* **2015**, *119*, 14938–14946, DOI: 10.1021/acs.jpcc.5b03538.

(6) Li, X.; Masters, A. F.; Maschmeyer, T. Photocatalytic Hydrogen Evolution from Silica–Templated Polymeric Graphitic Carbon Nitride: Is the Surface Area Important? *ChemCatChem* **2015**, *7*, 121–126, DOI: 10.1002/cctc.201402567.

(7) Bhunia, M. K.; Melissen, S. T. A. G.; Parida, M. R.; Sarawade, P.; Basset, J.-M.; Anjum, D. H.; Mohammed, O. F.; Sautet, P.; Le Bahers, T.; Takanabe, K. Dendritic Tip-on Polytriazine-Based Carbon Nitride Photocatalyst with High Hydrogen Evolution Activity. *Chem. Mater.* **2015**, *27*, 8237–8247, DOI: 10.1021/acs.chemmater.5b02974.

(8) Lau, V. W.-H.; Moudrakovski, I.; Botari, T.; Weinberger, S.; Mesch, M. B.; Duppel, V.; Senker, J.; Blum, V.; Lotsch, B. V. Rational design of carbon nitride photocatalysts by identification of cyanamide defects as catalytically relevant sites. *Nat. Commun.* **2016**, *7*, 12165, DOI: 10.1038/ncomms12165.

(9) Kessler, F. K.; Zheng, Y.; Schwarz, D.; Merschjann, C.; Schnick, W.; Wang, X.; Bojdys, M. J. Functional carbon nitride materials – design strategies for electrochemical devices. *Nat. Rev. Mater.* **2017**, *2*, 17030, DOI: 10.1038/natrevmats.2017.30.

(10) Niu, P.; Zhang, L.; Liu, G.; Cheng, H.-M. Graphene-Like Carbon Nitride Nanosheets for Improved Photocatalytic Activities. *Adv. Funct. Mater.* **2012**, *22*, 4763–4770, DOI: 10.1002/adfm.201200922.

(11) Liu, J.; Liu, Y.; Liu, N.; Han, Y.; Zhang, X.; Huang, H.; Lifshitz, Y.; Lee, S.-T.; Zhong, J.; Kang, Z. Metal-Free

Efficient Photocatalyst for Stable Visible Water Splitting via a Two-Electron Pathway. *Science* **2015**, *347*, 970–974, DOI: 10.1126/science.aaa3145.

(12) Lin, L.; Ou, H.; Zhang, Y.; Wang, X. Tri-s-triazine-Based Crystalline Graphitic Carbon Nitrides for Highly Efficient Hydrogen Evolution Photocatalysis. *ACS Catal.* **2016**, *6*, 3921–3931, DOI: 10.1021/acscatal.6b00922.

(13) Chen, J.; Yang, D.; Song, D.; Jiang, J.; Ma, A.; Hu, M. Z.; Ni, C. Recent progress in enhancing solar-to-hydrogen efficiency. *J. Power Sources* **2015**, *280*, 649–666, DOI: 10.1016/j.jpowsour.2015.01.073.

(14) Algara-Siller, G.; Severin, N.; Chong, S. Y.; Björkman, T.; Palgrave, R. G.; Laybourn, A.; Antonietti, M.; Khimyak, Y. Z.; Krasheninnikov, A. V.; Rabe, J. P.; Kaiser, U.; Cooper, A. I.; Thomas, A.; Bojdys, M. J. Triazine-Based Graphitic Carbon Nitride: a Two-Dimensional Semiconductor. *Angew. Chemie* **2014**, *126*, 7580–7585, DOI: 10.1002/ange.201402191.

(15) Lotsch, B. V.; Döblinger, M.; Sehnert, J.; Seyfarth, L.; Senker, J.; Oeckler, O.; Schnick, W. Unmasking Melon by a Complementary Approach Employing Electron Diffraction, Solid-State NMR Spectroscopy, and Theoretical Calculations-Structural Characterization of a Carbon Nitride Polymer. *Chem. Eur. J.* **2007**, *13*, 4969–80, DOI: 10.1002/chem.200601759.

(16) Seyfarth, L.; Seyfarth, J.; Lotsch, B. V.; Schnick, W.; Senker, J. Tackling the Stacking Disorder of Melon-Structure Elucidation in a Semicrystalline Material. *Phys. Chem. Chem. Phys.* **2010**, *12*, 2227–2237, DOI: 10.1039/B919918G.

(17) Fina, F.; Callear, S. K.; Carins, G. M.; Irvine, J. T. S. Structural Investigation of Graphitic Carbon Nitride via XRD and Neutron Diffraction. *Chem. Mater.* **2015**, *27*, 2612–2618, DOI: 10.1021/acs.chemmater.5b00411.

(18) Tyborski, T.; Merschjann, C.; Orthmann, S.; Yang, F.; Lux-Steiner, M.-C.; Schedel-Niedrig, T. Crystal Structure of Polymeric Carbon Nitride and the Determination of its Process-Temperature-Induced Modifications. *J. Phys. Condens. Matter* **2013**, *25*, 395402, DOI: 10.1088/0953-8984/25/39/395402.

(19) Li, X.; Sergeyev, I. V.; Aussenac, F.; Masters, A. F.; Maschmeyer, T.; Hook, J. M. Dynamic Nuclear Polarization NMR Spectroscopy of Polymeric Carbon Nitride Photocatalysts: Insights into Structural Defects and Reactivity. *Angew. Chem. online*, DOI: 10.1002/ange.201802278.

(20) Botari, T.; Huhn, W. P.; Lau, V. W.-H.; Lotsch, B. V.; Blum, V. Thermodynamic Equilibria in Carbon Nitride Photocatalyst Materials and Conditions for the Existence of Graphitic Carbon Nitride g-C_3N_4. *Chem. Mater.* **2017**, *29*, 4445–4453, DOI: 10.1021/acs.chemmater.7b00965.

(21) Melissen, S. T. A. G.; Steinmann, S. N.; Le Bahers, T.; Sautet, P. DFT Perspective on the Thermochemistry of Carbon Nitride Synthesis. *J. Phys. Chem. C* **2016**, *120*, 24542–24550, DOI: 10.1021/acs.jpcc.6b06335.

(22) Bredas, J.-L. Mind the gap! *Mater. Horiz.* **2014**, *1*, 17–19, DOI: 10.1039/C3MH00098B.

(23) Melissen, S.; Bahers, T. L.; Steinmann, S. N.; Sautet, P. Relationship between Carbon Nitride Structure and Exciton Binding Energies: A DFT Perspective. *J. Phys. Chem. C* **2015**, *119*, 25188–25196, DOI: 10.1021/acs.jpcc.5b07059.

(24) Niu, P.; Yin, L.-C.; Yang, Y.-Q.; Liu, G.; Cheng, H.-M. Increasing the Visible Light Absorption of Graphitic Carbon Nitride (Melon) Photocatalysts by Homogeneous

Self-Modification with Nitrogen Vacancies. *Adv. Mater.* **2014**, *26*, 8046–8052, DOI: 10.1002/adma.201404057.

(25) Perdew, J. P.; Burke, K.; Ernzerhof, M. Generalized Gradient Approximation Made Simple. *Phys. Rev. Lett.* **1996**, *77*, 3865–3868, DOI: 10.1103/PhysRevLett.77.3865.

(26) Perdew, J. P.; Burke, K.; Ernzerhof, M. Erratum: Generalized Gradient Approximation Made Simple [Phys. Rev. Lett. 77, 3865 (1996)]. *Phys. Rev. Lett.* **1997**, *78*, 1396–1396, DOI: 10.1103/PhysRevLett.78.1396.

(27) Steinmann, S. N.; Melissen, S. T. A. G.; Le Bahers, T.; Sautet, P. Challenges in Calculating the Bandgap of Triazine-Based Carbon Nitride Structures. *J. Mater. Chem. A* **2017**, *5*, 5115–5122, DOI: 10.1039/C6TA08939A.

(28) Merschjann, C.; Tyborski, T.; Orthmann, S.; Yang, F.; Schwarzburg, K.; Lublow, M.; Lux-Steiner, M.-C.; Schedel-Niedrig, T. Photophysics of polymeric carbon nitride: An optical quasimonomer. *Phys. Rev. B* **2013**, *87*, 205204, DOI: 10.1103/PhysRevB.87.205204.

(29) Butchosa, C.; Guiglion, P.; Zwijnenburg, M. A. Carbon Nitride Photocatalysts for Water Splitting: A Computational Perspective. *J. Phys. Chem. C* **2014**, *118*, 24833–24842, DOI: 10.1021/jp507372n.

(30) Lau, V. W.-H.; Mesch, M. B.; Duppel, V.; Blum, V.; Senker, J.; Lotsch, B. V. Low-Molecular-Weight Carbon Nitrides for Solar Hydrogen Evolution. *J. Am. Chem. Soc.* **2015**, *137*, 1064–1072, DOI: 10.1021/ja511802c.

(31) Zambon, A.; Mouesca, J.-M.; Gheorghiu, C.; Bayle, P. A.; Pecaut, J.; Claeys-Bruno, M.; Gambarelli, S.; Dubois, L. s-Heptazine Oligomers: Promising Structural Models for Graphitic Carbon Nitride. *Chem. Sci.* **2016**, *7*, 945–950, DOI: 10.1039/C5SC02992A.

(32) Kang, Y.; Yang, Y.; Yin, L.-C.; Kang, X.; Liu, G.; Cheng, H.-M. An Amorphous Carbon Nitride Photocatalyst with Greatly Extended Visible-Light-Responsive Range for Photocatalytic Hydrogen Generation. *Adv. Mater.* **2015**, *27*, 4572–4577, DOI: 10.1002/adma.201501939.

(33) Fabian, D. M.; Hu, S.; Singh, N.; Houle, F. A.; Hisatomi, T.; Domen, K.; Osterloh, F. E.; Ardo, S. Particle suspension reactors and materials for solar-driven water splitting. *Energy Environ. Sci.* **2015**, *8*, 2825–2850, DOI: 10.1039/C5EE01434D.

(34) Ong, W.-J.; Tan, L.-L.; Ng, Y. H.; Yong, S.-T.; Chai, S.-P. Graphitic Carbon Nitride (g-C_3N_4)-Based Photocatalysts for Artificial Photosynthesis and Environmental Remediation: Are We a Step Closer To Achieving Sustainability? *Chem. Rev.* **2016**, *116*, 7159–7329, DOI: 10.1021/acs.chemrev.6b00075.

(35) Schwarzer, A.; Saplinova, T.; Kroke, E. Tri-*s*-triazines (s-heptazines) - From a "mystery molecule" to industrially relevant carbon nitride materials. *Coordin. Chem. Rev.* **2013**, *257*, 2032–2062, DOI: 10.1016/j.ccr.2012.12.006.

(36) Adamo, C.; Jacquemin, D. The calculations of excited-state properties with Time-Dependent Density Functional Theory. *Chem. Soc. Rev.* **2013**, *42*, 845–856, DOI: 10.1039/C2CS35394F.

(37) Grimme, S.; Neese, F. Double-hybrid density functional theory for excited electronic states of molecules. *J. Chem. Phys.* **2007**, *127*, 154116, DOI: 10.1063/1.2772854.

(38) Grimme, S. Semiempirical hybrid density functional with perturbative second-order correlation. *J. Chem. Phys.* **2006**, *124*, 034108, DOI: 10.1063/1.2148954.

(39) Dunning, J., Thom H. Gaussian basis sets for use in correlated molecular calculations. I. The atoms boron through neon and hydrogen. *J. Chem. Phys.* **1989**, *90*, 1007–1023, DOI: 10.1063/1.456153.

(40) Neese, F. The ORCA program system. *WIREs Comput Mol Sci* **2012**, *2*, 73–78, DOI: 10.1002/wcms.81.

(41) Goerigk, L.; Grimme, S. Double-hybrid density functionals. *Wiley Interdiscip. Rev. Comput. Mol. Sci. 4*, 576–600, DOI: 10.1002/wcms.1193.

(42) Prlj, A.; Sandoval-Salinas, M. E.; Casanova, D.; Jacquemin, D.; Corminboeuf, C. Low-Lying π-π* States of Heteroaromatic Molecules: A Challenge for Excited State Methods. *J. Chem. Theory Comput.* **2016**, *12*, 2652–2660, DOI: 10.1021/acs.jctc.6b00245.

(43) Goerigk, L.; Moellmann, J.; Grimme, S. Computation of accurate excitation energies for large organic molecules with double-hybrid density functionals. *Phys. Chem. Chem. Phys.* **2009**, *11*, 4611–4620, DOI: 10.1039/B902315A.

(44) Jorge, A. B.; Martin, D. J.; Dhanoa, M. T. S.; Rahman, A. S.; Makwana, N.; Tang, J.; Sella, A.; Corà, F.; Firth, S.; Darr, J. A.; McMillan, P. F. H_2 and O_2 Evolution from Water Half-Splitting Reactions by Graphitic Carbon Nitride Materials. *J. Phys. Chem. C* **2013**, *117*, 7178–7185, DOI: 10.1021/jp4009338.

(45) Sing, K. S. Adsorption Methods for the Characterization of Porous Materials. *Adv. Colloid Interface Sci.* **1998**, *76-77*, 3–11, DOI: 10.1016/S0001-8686(98)00038-4.

(46) Varshni, Y. Temperature Dependence of the Energy Gap in Semiconductors. *Physica* **1967**, *34*, 149–154, DOI: 10.1016/0031-8914(67)90062-6.

(47) O'Donnell, K.-P.; Chen, X. Temperature dependence of semiconductor band gaps. **1991**, *58*, 2924–2926, DOI: 10.1063/1.104723.

(48) Allen, P. B.; Heine, V. Theory of the temperature dependence of electronic band structures. *J. Phys. C Solid State Phys.* **1976**, *9*, 2305–2312, DOI: 10.1088/0022-3719/9/12/013.

(49) Jiang, X.-D.; Guan, J.; Zhao, J.; Guennic, B. L.; Jacquemin, D.; Zhang, Z.; Chen, S.; Xiao, L. Synthesis, Structure and Photophysical Properties of NIR Aza-BODIPYs with -F/-N_3/-NH_2 Groups at 1,7-Positions. *Dyes and Pigments* **2017**, *136*, 619–626, DOI: 10.1016/j.dyepig.2016.09.019.

(50) Venkataraman, K. *The Chemistry of Synthetic Dyes, Volume IV*; Academic Press New York, N.Y, 1971.

(51) Jin, X.; Balasubramanian, V.; Selvan, S.; Sawant, D.; Chari, M.; Lu, G.; Vinu, A. Highly Ordered Mesoporous Carbon Nitride Nanoparticles with High Nitrogen Content: A Metal-Free Basic Catalyst. *Angew. Chem. 121*, 8024–8027, DOI: 10.1002/ange.200903674.

(52) Lau, V. W.-H.; Yu, V. W.-Z.; Ehrat, F.; Botari, T.; Moudrakovski, I.; Simon, T.; Duppel, V.; Medina, E.; Stolarczyk, J. K.; Feldmann, J.; Blum, V.; Lotsch, B. V. Urea-Modified Carbon Nitrides: Enhancing Photocatalytic Hydrogen Evolution by Rational Defect Engineering. *Adv. Energy Mater.* **2017**, *7*, 1602251, DOI: 10.1002/aenm.201602251.

(53) Döblinger, M.; Lotsch, B. V.; Wack, J.; Thun, J.; Senker, J.; Schnick, W. Structure Elucidation of Polyheptazine Imide by Electron Diffraction a Templated 2D Carbon Nitride Network. *Chem. Commun.* **2009**, 1541–1543, DOI: 10.1039/B820032G.

(54) Sk, M. A.; Ananthanarayanan, A.; Huang, L.; Lim, K. H.; Chen, P. Revealing the tunable photoluminescence

properties of graphene quantum dots. *J. Mater. Chem. C* **2014**, *2*, 6954–6960, DOI: 10.1039/C4TC01191K.